

Modified Winterbottom Construction Including Boundaries

Zachary R. Mansley and Laurence D. Marks*



Cite This: *J. Phys. Chem. C* 2020, 124, 28038–28043



Read Online

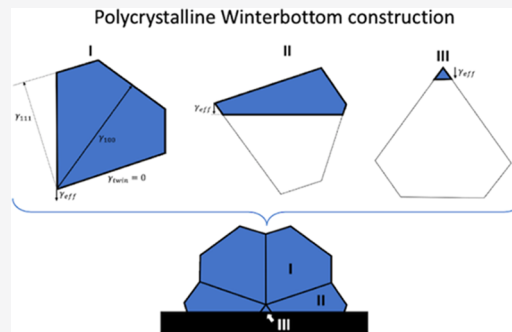
ACCESS |

Metrics & More

Article Recommendations

Supporting Information

ABSTRACT: There has been extensive work on the equilibrium shape of isolated nanoparticles with internal boundaries and also single crystals on substrates. Surprisingly, almost shockingly, there has been very little work on the equilibrium shape of particles with internal boundaries on substrates. Here, the general solution is given for the configuration of particles containing twin and other grain boundaries on a flat substrate, which can be applied to any polycrystalline or multiphase nanoparticle configuration. The solution is based upon combining the established modified Wulff construction that has been extensively validated for twinned particles with the Winterbottom construction for single particles on a substrate. The solution is illustrated for the specific case of five-fold multiply twinned particles (MTPs). Good agreement is observed between both existing experimental data in the literature as well as some experimental data included within this work.



INTRODUCTION

Nanoparticles have seen a significant amount of research interest in the 21st century. They can be engineered with specific compositions^{1–3} and shapes^{4–6} and have applications in many areas such as catalysis^{7–11} and medicine.^{12–16} Controlling the shape and morphology of nanoparticles is particularly interesting, as it allows for a significant degree of optimization for specific uses, such as reactions that only occur on specific crystal facets.^{17,18} This is only achievable with a thorough understanding of these systems and their thermodynamics.

Nanoparticles can be single crystalline, Janus-type,^{19,20} core–shell,²¹ polycrystalline, or multiply twinned particles (MTPs).²² The thermodynamics and competing energetics that define the different types have been well studied for freestanding nanoparticles,^{22–26} but a significant portion of nanoparticle applications require stabilization, where the nanoparticle is supported on a substrate.^{2,3,7,8,13,14,27} The thermodynamic description of supported single crystals is the Winterbottom construction, which is an extension of the thermodynamic Wulff construction.^{28–32} However, the Winterbottom construction is limited to single-crystal particles.²⁸ Here we expand the Winterbottom construction to include multiple crystallographic units in the supported particle and use an anisotropic 5-fold MTP as a test case to illustrate this expanded model, as well as presenting experimental examples.

METHODS

For the experimental data, oxide substrates were synthesized using a hydro-sauna method for producing faceted, rare-earth scandate nanoparticles.^{33,34} Au nanoparticles were prepared on these substrates using a deposition precipitation reaction, as

described by Zanella et al.³⁵ Transmission electron microscopy (TEM) was performed using a JEOL ARM300F operated at 300 kV located at the NUANCE center at Northwestern University and on the Argonne Chromatic Aberration-corrected TEM (ACAT) operated at 200 kV at the Center for Nanoscale Materials in Argonne National Lab.

RESULTS AND DISCUSSION

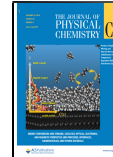
Supported MTPs of Au were observed, as shown in Figure 1, and more examples from both this material system and from other literature sources can be found in the Supporting Information. The majority of the Au nanoparticles are observed to be twinned at small sizes and single crystalline at larger sizes (see Figure S1), which is consistent with thermodynamic predictions for MTP energetics.^{22,26}

As previously demonstrated by Marks^{24–26} in what he called a “Modified Wulff construction”, the underlying process of solving for the thermodynamic shape is very similar for MTPs and single crystals. Assuming that the particle is symmetric, for a freestanding MTP where the surface free energy as a function of the crystallographic normal direction \hat{n} is $\gamma_s(\hat{n})$, one would first plot this in three dimensions, generate a plane normal to the radii at each point, and finally use the inner envelope shape generated as the Wulff construction.^{30–32} To account for the twin boundaries, an internal interfacial term $\gamma_t(\hat{n})$ is included

Received: August 10, 2020

Revised: October 26, 2020

Published: December 9, 2020



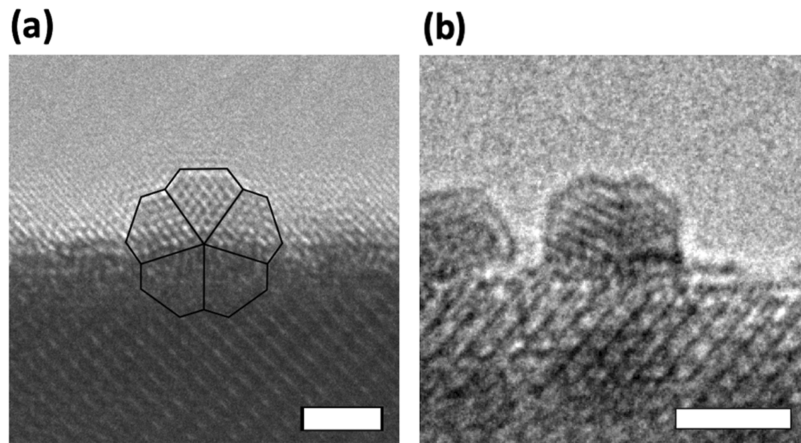


Figure 1. Experimental TEM image of 5-fold Au MTPs supported on faceted LnScO_3 nanoparticles^{33,34} containing re-entrant surfaces with the shape overlaid in (a) for clarity. The inverted orientation is shown in (b). The scale bar is 2 nm.

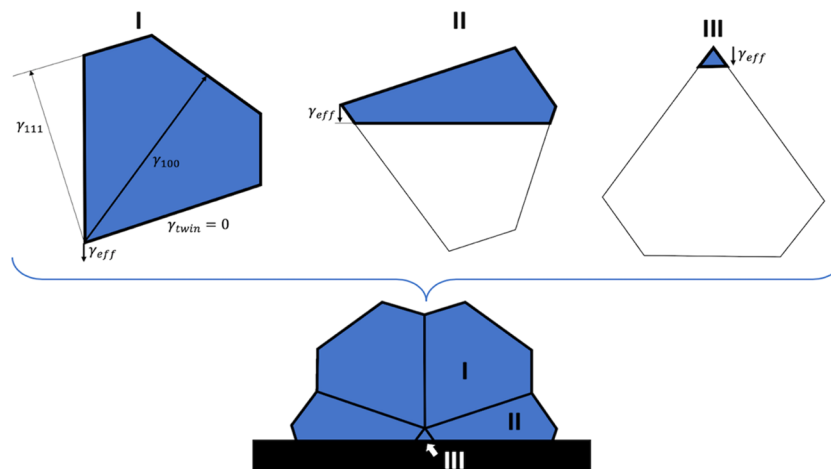


Figure 2. Winterbottom construction for an MTP. Segment I shows the generation of the crystallite segment for a 5-fold MTP along the [110] view direction. Here, the twin boundary energy is 0 so the twin facets pass through the Wulff center. Adding the interfacial energy in the direction of the interface relative to each particle segment yields the supported particle.

along with appropriate symmetry-defined constraints on the twin geometries.^{24–26} This is shown schematically in segment I in Figure 2.

Now we add a substrate to a symmetric, freestanding nanoparticle, assume that the support interface is flat (a necessary assumption), and specify the relative orientation of the nanoparticle and substrate. (In general, there is an additional degree of freedom associated with rotation of the nanoparticle.) The substrate introduces an additional effective interface energy γ_{eff} for the different segments of an MTP. While each crystallite has its own local orientation, the (flat) substrate interface is global, so it impacts each segment differently as described by Figure 2. Oriented as shown, the 5 crystallite components of the MTP now fall into 3 unique shapes. In the case of segment I, γ_{eff} is outside of the minimum energy Wulff shape leaving the crystallite unchanged, but for II and III, it creates a new interface.

We define the effective interface term, γ_{eff} such that it will vary with height (h) as the relative areal contributions of each crystallite change

$$\gamma_{\text{eff}}(h) = \sum_i \gamma_i(\hat{n}) f_i(h) \quad (1)$$

where γ_i is the local interfacial energy between segment i and the support and f_i is the fraction of the total interfacial area (A_{int}) of each segment such that $A_{\text{int}} f_i = A_i$, the areal contribution of each independent crystallite i . A sufficient condition for a local minimum is the minimization of surface energies, which can be expressed as^{22,36,37}

$$S = x: x \cdot \hat{n} \leq \lambda \gamma(\hat{n}) \quad (2)$$

where S represents the set of points that make up the shape of the particle and encompasses all points in a given normal direction that are less than the product of the surface energy in that direction and a volumetric constant λ . This deviates from the modified Wulff construction as, in the direction of the interface, $\gamma(\hat{n}) = \gamma_{\text{eff}}$. This substitution is justified in Appendix I and II of the Supporting Information. Note that this is only a sufficient condition; as we will see, there can be other local minima as the problem is not analytically continuous.

To analyze the energies further, it is useful to introduce a dimensionless parameter to represent the excess surface energy independent of volume (ϵ_w)^{24–26}

$$\epsilon_w = \frac{1}{\gamma_{111}} \left(\int dV \right)^{2/3} \quad (3)$$

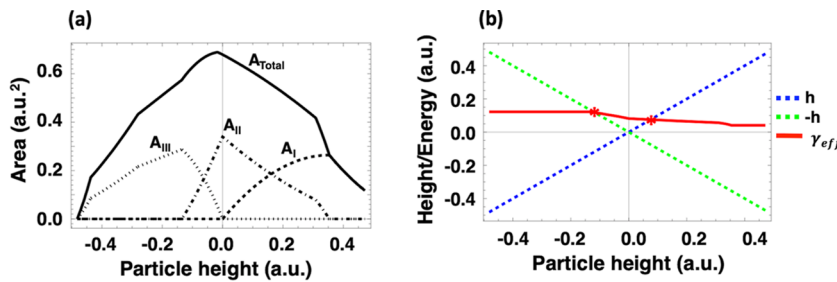


Figure 3. Contributions of each crystallite to the total interfacial area are shown in (a) using the notation and segment numbering from Figure 2. The plot in (b) shows the effective interfacial energy against height, where the intersections represent low-energy solutions for the MTP. Both h and $-h$ are plotted to represent the two possible inverted orientations of the nanoparticle with the defined interface. Moving from single crystals to polycrystals removes inversion symmetry (if it was present) and both orientations must be assessed.

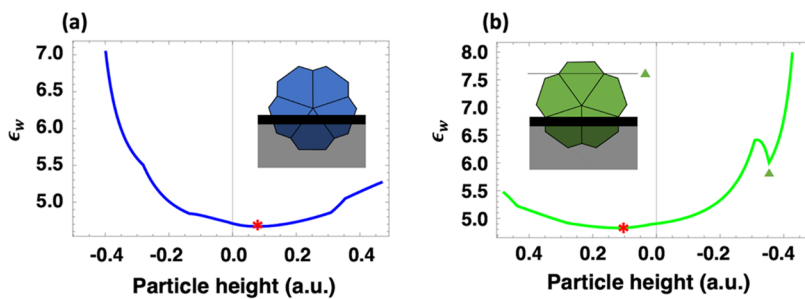


Figure 4. Energy calculations for inverted orientations of the same particle are shown in (a) and (b), with their minimum values indicated in red; these can be compared to the experimental images in Figure 1. There is an energetic local minimum in (b) indicated with a triangle. Note the sign of the x axis in (b).

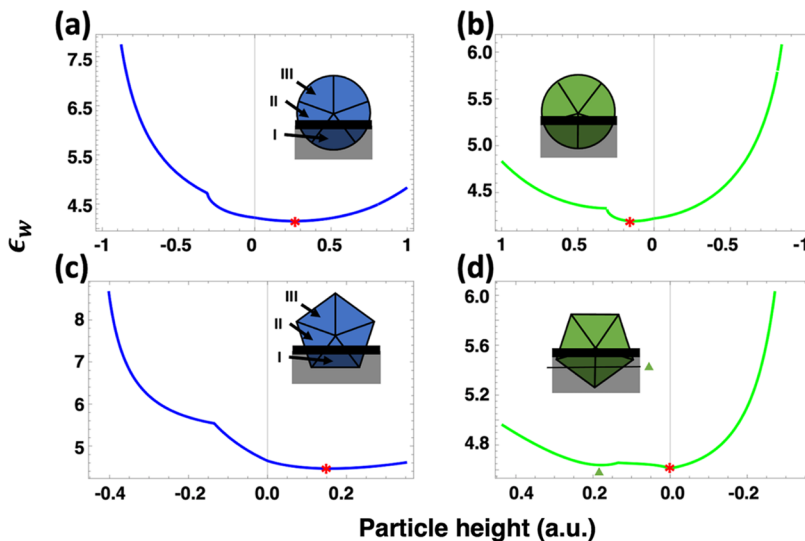


Figure 5. ϵ_w Plots for different 5-fold MTP geometries. (a) and (b) show an isotropic particle where $\gamma(\hat{n}) = 1$ and the interfacial energies of segments I, II, and III have been set to 0.1, 0.2, and 0.3, respectively. In (c) and (d), we set $\gamma_{100} = \frac{\sqrt{3}}{2} \gamma_{111}$, the energy ratio at which the re-entrant surfaces disappear from the MTP edges. The interfacial energies are set to 0.3, 0.4, and 0.5 times γ_{100} (now the lowest-energy external face) for segments I, II, and III, respectively. Absolute minima are indicated in red, and the triangle indicates a local minima.

where V is the total volume of the particle and γ_{111} is the surface energy of the (111) face (this has a number of useful properties and is briefly discussed further in Appendix II.) The general form includes the twin boundary energies, but these are small compared to surface energies in most fcc metals, so a good approximation is to neglect the twin boundary energy.²⁴ In principle, the strain in the particles from both the misfit with the substrate and the angular deficit in MTPs should be included in the surface and interface energy terms, as discussed

previously.^{22,26} Specific calculations indicate that the effect is generally small.^{38,39} It should also be noted that the misfit strain with the substrate will be dependent on the material system of choice and the interaction of this misfit with the angular deficit for various systems is of interest for future study.

Using these terms, a modified Winterbottom construction for MTPs can be generated using the following steps:

- (1) Evaluate γ_{eff} (h) and find intersections where γ_{eff} (h) = h or the distance from the Wulff center. As described in

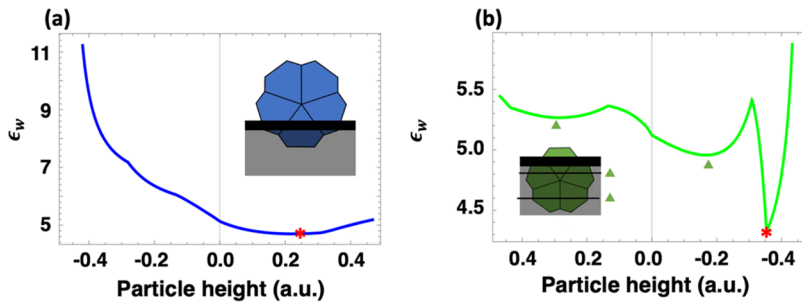


Figure 6. ϵ_w plots using the same external energies as the particle in Figures 3 and 4, with the interfacial energies changed $-0.2, 0.4$, and $0.7 \gamma_{111}$. As shown, the impact on the plots and the location of the minima is significant when compared to changes arising from differences in the external energies.

Appendix I, this represents the minimum energy Wulff condition.

- (2) Calculate ϵ_w to find the lowest-energy orientation and any other local minima.

We will now apply this model to a theoretical 5-fold MTP with an interface oriented as shown in Figure 2, and discuss the results. As a simplified model, we will assume a strongly faceted fcc metal nanoparticle with {111}- and {100}-type faces, a twin boundary energy of zero, and a broken bond approach to the surface such that $\gamma_{100} = \frac{2}{\sqrt{3}} \gamma_{111}$. While these terms are chosen for simplicity and convenience of explanation, this framework can be applied to noncubic materials with different values of γ_{hkl} with appropriate symmetry considerations.

The contributions to the overall interfacial area from each crystallite type (I, II, and III) can be calculated as a function of height, as shown in Figure 3a. To calculate γ_{eff} , we now assign arbitrary interfacial energy values to each interface: 0.1, 0.2, and 0.3 times γ_{111} for segments I, II, and III, respectively. Plotting this against the particle height, as shown in Figure 3b, gives low-energy solutions for the 5-fold particle given this set of interfacial energies.

Figure 4 shows ϵ_w for the two orientations of the same planar interface. The absolute minimum for each plot occurs where $\gamma_{eff} = h$, confirming the minimum energy solution. Evaluating ϵ_w at these minima gives values of 4.67 and 4.83 for the orientations shown in Figure 4a and 4b meaning that the morphology in Figure 4a is of lower energy given the input parameters. These two solutions correlate well with the experimental results shown in Figure 1. In addition, it can be seen in Figure 4b that there is a local minimum owing to the discontinuous change when the interface moves from being only in one segment to involving three (this can be compared to the case for a particle with lamellar twin boundaries shown in Figure S5 where no such discontinuities will arise).

One can insert experimental values for surface energies of commonly used metals (Au, Ag, Pd, etc.) into this model rather than using an arbitrary value along with the broken bond approach for a strongly faceted particle, but the overall shape of these curves remains similar with the location of the energetic minima only shifting slightly. Examples of other 5-fold morphologies are shown in Figure 5, where Figure 5a/b demonstrate isotropic surface energies and Figure 5c/d show the case when there are no re-entrant (111) planes at the twin boundaries. It can be seen that the locations of the minima are not significantly changed, though the relative energies at each are different as the external surface energies are changed;

furthermore, the discontinuity near -0.4 in Figure 4b has disappeared since it was a product of the notches characteristic of the Marks decahedron.

In the case of Figure 5d, the local minima at the origin that arises from the intersection of the 5 twin boundaries has become the lowest energy. The minima near 0.2 here occurs at an intersection with crystal segment III, and the higher interfacial energy of that segment drives the energy of the entire particle up. To compare the impact of changing the external energies versus the interfacial energies, we take the model from Figure 4 and make changes to the interfacial energies while leaving the external energies constant, and the result is shown in Figure 6. As demonstrated, the effect of changing the interfacial energies has a greater impact on the energy landscape and degree of truncation of the nanoparticle than changing the external surface energies.

The modified Winterbottom solution for MTPs on substrates is somewhat simple; one has to extend from the normal solution and solve for an additional constraint involving the effective interfacial free energy. As such, this is similar to the additional constraints required to solve for alloy nanoparticles.⁴⁰ Because in general it will be impossible to simultaneously have strong adhesion for all of the different single-crystal units with the substrate, the adhesion will always be smaller (e.g., see Figure S2) than a single crystal. Additionally, it is these interfacial energies that predominantly define the truncation height and the location of the energetic minima in the ϵ_w calculations (Figure 6), as is the case with the single-crystalline Winterbottom construction. One important point to note is the intersection of the twin boundaries themselves with the substrate. We have assumed a twin energy of zero and by extension no interaction between said boundary and the support surface; however, this will not be the case in reality, where this will be energetically positive.

The model presented thus far is purely thermodynamic, as we have used the nominal surface energies in vacuum to define the Wulff construction. Particle shapes and growth can also be defined kinetically, where the growth velocity of a facet is used rather than the energy.^{22,30} As a result, if these polycrystalline particles are formed on the substrate in a kinetic manner (as opposed to allowed to reach local equilibrium), then the Wulff center will necessarily intersect with the substrate as the interface with the substrate has a growth velocity of zero. However, it is rarely the case where a growth will be entirely thermodynamic or kinetic, instead a mix of the two factors is expected. An experimentally observed example of kinetic influence, as well as local minima from faceting discontinuity, can be seen in Figure S2.

While we have here described the specific case for a 5-fold MTP, the solution is quite general. It can be applied to lamellar-twinned particles with one or more parallel twin boundaries (Figure S5) or more complex MTPs such as icosahedra (Figure S3), as well as Janus-type particles, multicomponent particles, or any other case where the nanoparticle on the support contains more than one distinct crystallographic unit. In the examples shown in the Supporting Information, as well as the tilted 5-fold example in Figure S4, the particle morphology is such that low-energy facets form the interface with the support to minimize γ_{eff} . Asymmetric MTPs can also be described with this model and appropriate volumetric scaling, but the kinetic factors involved in their formation make them difficult to predict from a thermodynamic standpoint.

CONCLUSIONS

The general thermodynamic shape of supported polycrystalline nanoparticles can be described by combining the established modified Wulff construction and the Winterbottom construction.

ASSOCIATED CONTENT

Supporting Information

The Supporting Information is available free of charge at <https://pubs.acs.org/doi/10.1021/acs.jpcc.0c07316>.

Mathematical proofs of the surface energy minimization and the substitution of γ_{eff} for individual segments along with experimental example images ([PDF](#))

AUTHOR INFORMATION

Corresponding Author

Laurence D. Marks — Department of Materials Science and Engineering, Northwestern University, Evanston, Illinois 60206, United States; Email: l-marks@northwestern.edu

Author

Zachary R. Mansley — Department of Materials Science and Engineering, Northwestern University, Evanston, Illinois 60206, United States; orcid.org/0000-0002-1284-6316

Complete contact information is available at:

<https://pubs.acs.org/10.1021/acs.jpcc.0c07316>

Author Contributions

The manuscript was conceived and written through the contributions of all authors. All authors have given approval to the final version of the manuscript.

Funding

Z.R.M. was supported by the Northwestern University Institute for Catalysis in Energy Processes (ICEP) with Grant No. DOE DE-FG02-03ER15457. L.D.M. acknowledges the partial support by the National Science Foundation (NSF) under grant number DMR-1507101.

Notes

The authors declare no competing financial interest.

ACKNOWLEDGMENTS

We acknowledge the use of the Center for Nanoscale Materials, a user facility at the Argonne National Lab supported by the U.S. Department of Energy, Office of Science, Office of Basic Energy Sciences, under Contract No.

DE-AC02-06CH11357. We thank Dr. R.J. Paull for synthesizing the oxide supports, Dr. A. Gosavi for the Au preparation, and Prof. P. Voorhees for the useful comments.

REFERENCES

- (1) Ferrando, R.; Jellinek, J.; Johnston, R. L. Nanoalloys: From Theory to Applications of Alloy Clusters and Nanoparticles. *Chem. Rev.* **2008**, *108*, 845–910.
- (2) Park, J. Y.; Zhang, Y.; Grass, M.; Zhang, T.; Somorjai, G. A. Tuning of Catalytic Co Oxidation by Changing Composition of Rh-Pt Bimetallic Nanoparticles. *Nano Lett.* **2008**, *8*, 673–677.
- (3) Park, J. B.; Conner, S. F.; Chen, D. A. Bimetallic Pt-Au Clusters on TiO₂(110): Growth, Surface Composition, and Metal-Support Interactions. *J. Phys. Chem. C* **2008**, *112*, 5490–5500.
- (4) Nguyen, T. D. From Formation Mechanisms to Synthetic Methods toward Shape-Controlled Oxide Nanoparticles. *Nanoscale* **2013**, *5*, 9455–9482.
- (5) Xia, Y. N.; Xiong, Y. J.; Lim, B.; Skrabalak, S. E. Shape-Controlled Synthesis of Metal Nanocrystals: Simple Chemistry Meets Complex Physics? *Angew. Chem., Int. Ed.* **2009**, *48*, 60–103.
- (6) Dong, L. Q.; Shi, H.; Cheng, K.; Wang, Q.; Weng, W. J.; Han, W. Q. Shape-Controlled Growth of SrTiO₃ Polyhedral Submicro/Nanocrystals. *Nano Res.* **2014**, *7*, 1311–1318.
- (7) Enterkin, J. A.; Setthapun, W.; Elam, J. W.; Christensen, S. T.; Rabuffetti, F. A.; Marks, L. D.; Stair, P. C.; Poeppelmeier, K. R.; Marshall, C. L. Propane Oxidation over Pt/SrTiO₃ Nanocuboids. *ACS Catal.* **2011**, *1*, 629–635.
- (8) Enterkin, J. A.; Poeppelmeier, K. R.; Marks, L. D. Oriented Catalytic Platinum Nanoparticles on High Surface Area Strontium Titanate Nanocuboids. *Nano Lett.* **2011**, *11*, 993–7.
- (9) Enterkin, J. A.; Kennedy, R. M.; Lu, J. L.; Elam, J. W.; Cook, R. E.; Marks, L. D.; Stair, P. C.; Marshall, C. L.; Poeppelmeier, K. R. Epitaxial Stabilization of Face Selective Catalysts. *Top. Catal.* **2013**, *56*, 1829–1834.
- (10) Haruta, M. When Gold Is Not Noble: Catalysis by Nanoparticles. *Chem. Rec.* **2003**, *3*, 75–87.
- (11) Chen, B.-R.; et al. Morphology and Co Oxidation Activity of Pd Nanoparticles on SrTiO₃ Nanopolyhedra. *ACS Catal.* **2018**, *8*, 4751–4760.
- (12) Zhang, L. N.; Deng, H. H.; Lin, F. L.; Xu, X. W.; Weng, S. H.; Liu, A. L.; Lin, X. H.; Xia, X. H.; Chen, W. In Situ Growth of Porous Platinum Nanoparticles on Graphene Oxide for Colorimetric Detection of Cancer Cells. *Anal. Chem.* **2014**, *86*, 2711–2718.
- (13) Neupane, M. P.; Park, I. S.; Bae, T. S.; Yi, H. K.; Uo, M.; Watari, F.; Lee, M. H. Titania Nanotubes Supported Gelatin Stabilized Gold Nanoparticles for Medical Implants. *J. Mater. Chem.* **2011**, *21*, 12078–12082.
- (14) Malakootian, M.; Nasiri, A.; Gharaghani, M. A. Photocatalytic Degradation of Ciprofloxacin Antibiotic by TiO₂ Nanoparticles Immobilized on a Glass Plate. *Chem. Eng. Commun.* **2020**, *207*, 56–72.
- (15) Sridhar, R.; Lakshminarayanan, R.; Madhaiyan, K.; Barathi, V. A.; Limh, K. H. C.; Ramakrishna, S. Electrosprayed Nanoparticles and Electrospun Nanofibers Based on Natural Materials: Applications in Tissue Regeneration, Drug Delivery and Pharmaceuticals. *Chem. Soc. Rev.* **2015**, *44*, 790–814.
- (16) Wadajkar, A. S.; et al. Prostate Cancer-Specific Thermoresponsive Polymer-Coated Iron Oxide Nanoparticles. *Biomaterials* **2013**, *34*, 3618–3625.
- (17) Lin, H. F.; Li, L. P.; Zhao, M. L.; Huang, X. S.; Chen, X. M.; Li, G. S.; Yu, R. C. Synthesis of High-Quality Brookite TiO₂ Single-Crystalline Nanosheets with Specific Facets Exposed: Tuning Catalysts from Inert to Highly Reactive. *J. Am. Chem. Soc.* **2012**, *134*, 8328–8331.
- (18) Bi, Y.; Ouyang, S.; Umezawa, N.; Cao, J.; Ye, J. Facet Effect of Single-Crystalline Ag₃Po₄ Sub-Micromaterials on Photocatalytic Properties. *J. Am. Chem. Soc.* **2011**, *133*, 6490–6492.

- (19) de Gennes, P. G. Soft Matter (Nobel Lecture). *Angew. Chem., Int. Ed.* **1992**, *31*, 842–845.
- (20) Lattuada, M.; Hatton, T. A. Synthesis, Properties and Applications of Janus Nanoparticles. *Nano Today* **2011**, *6*, 286–308.
- (21) Ghosh Chaudhuri, R.; Paria, S. Core/Shell Nanoparticles: Classes, Properties, Synthesis Mechanisms, Characterization, and Applications. *Chem. Rev.* **2012**, *112*, 2373–2433.
- (22) Marks, L. D.; Peng, L. Nanoparticle Shape, Thermodynamics and Kinetics. *J. Phys.: Condens. Matter* **2016**, *28*, No. 053001.
- (23) Ino, S.; Ogawa, S. Multiply Twinned Particles at Earlier Stages of Gold Film Formation on Alkalihalide Crystals. *J. Phys. Soc. Jpn.* **1967**, *22*, 1365–1374.
- (24) Marks, L. D. Surface-Structure and Energetics of Multiply Twinned Particles. *Philos. Mag. A* **1984**, *49*, 81–93.
- (25) Marks, L. D. Modified Wulff Constructions for Twinned Particles. *J. Cryst. Growth* **1983**, *61*, 556–566.
- (26) Howie, A.; Marks, L. D. Elastic Strains and the Energy-Balance for Multiply Twinned Particles. *Philos. Mag. A* **1984**, *49*, 95–109.
- (27) Enterkin, J. A.; Kennedy, R. M.; Lu, J.; Elam, J. W.; Cook, R. E.; Marks, L. D.; Stair, P. C.; Marshall, C. L.; Poeppelmeier, K. R. Epitaxial Stabilization of Face Selective Catalysts. *Top. Catal.* **2013**, *56*, 1829–1834.
- (28) Winterbottom, W. L. Equilibrium Shape of a Small Particle in Contact with a Foreign Substrate. *Acta Metall.* **1967**, *15*, 303–310.
- (29) Zia, R. K. P.; Avron, J. E.; Taylor, J. E. The Summertop Construction - Crystals in a Corner. *J. Stat. Phys.* **1988**, *50*, 727–736.
- (30) Wulff, G. On the Question of Speed of Growth and Dissolution of Crystal Surfaces. *Z. Krystallogr. Mineral.* **1901**, *34*, 449–530.
- (31) Dinghas, A. On Wulff's Geometric Theorem for the Balanced Form of Crystals. *Z. Krystallogr.* **1944**, *105*, 304–314.
- (32) Laue, M. V. Der Wulffsche Satz Für Die Gleichgewichtsform Von Kristallen. *Z. Krystallogr.* **1943**, *105*, 124–133.
- (33) Paull, R. J.; Mansley, Z. R.; Ly, T.; Marks, L. D.; Poeppelmeier, K. R. Synthesis of Gadolinium Scandate from a Hydroxide Hydrogel. *Inorg. Chem.* **2018**, *57*, 4104–4108.
- (34) Paull, R. J.; Ly, T.; Mansley, Z. R.; Poeppelmeier, K. R.; Marks, L. D. Controlled Two-Step Formation of Faceted Perovskite Rare-Earth Scandate Nanoparticles. *Crystals* **2019**, *9*, 218.
- (35) Zanella, R.; Giorgio, S.; Shin, C. H.; Henry, C. R.; Louis, C. Characterization and Reactivity in Co Oxidation of Gold Nanoparticles Supported on TiO₂ Prepared by Deposition-Precipitation with NaOH and Urea. *J. Catal.* **2004**, *222*, 357–367.
- (36) Hoffman, D. W.; Cahn, J. W. Vector Thermodynamics for Anisotropic Surfaces. 1. Fundamentals and Application to Plane Surface Junctions. *Surf. Sci.* **1972**, *31*, 368–388.
- (37) Cahn, J. W.; Hoffman, D. W. Vector Thermodynamics for Anisotropic Surfaces. 2. Curved and Faceted Surfaces. *Acta Metall.* **1974**, *22*, 1205–1214.
- (38) Patala, S.; Marks, L. D.; de la Cruz, M. O. Elastic Strain Energy Effects in Faceted Decahedral Nanoparticles. *J. Phys. Chem. C* **2013**, *117*, 1485–1494.
- (39) Patala, S.; Marks, L. D.; de la Cruz, M. O. Thermodynamic Analysis of Multiply Twinned Particles: Surface Stress Effects. *J. Phys. Chem. Lett.* **2013**, *4*, 3089–3094.
- (40) Ringe, E.; Van Duyne, R. P.; Marks, L. D. Wulff Construction for Alloy Nanoparticles. *Nano Lett.* **2011**, *11*, 3399–3403.